recent detection of η^2-coordinated C-H bonds by Bergman et al.[31]

Conclusions

The special arrangement of ligands in square-planar Ir[$C_6H_4(CH_2NMe_2)$-2](COD) has resulted in the isolation of unique adducts with organotin(IV) halides that can be regarded as "trapped" three-center intermediates in the oxidative addition of a metal-halide bond to metal d^8 complex. It can be anticipated, based on isolobal relationships, that many new transition-metal complexes having side-on coordinated (main group) M-X bonds can be synthesized not only with tin(IV) (or other group 14 elements) but also with d^{10} metals like thallium(III), mercury(II), and gold(I).

Acknowledgment. X-ray data were kindly collected by A. J. M. Duisenberg. This work was supported in part (W.J.J.S. and A.L.S.) by the Dutch Foundation for Chemical Research (SON) with financial aid from the Dutch Organization for Advancement of Pure Research (ZWO).

Registry No. 1, 115076-05-6; **2**, 115076-06-7; **3**, 115076-07-8; **4a**, 115076-08-9; **4b**, 115116-29-5; **5**, 115076-09-0; **6**, 115076-10-3; Ir[$C_6H_4(CH_2NMe_2)$-2](COD), 114762-91-3; $SnMe_2Cl_2$, 753-73-1; $SnMe_2Br_2$, 2767-47-7; $SnPh_2Cl_2$, 1135-99-5; $SnMePhBr_2$, 21247-36-9; $SnMeCl_3$, 993-16-8; $SnBr_4$, 7789-67-5; $[IrBr(COD)]_2$, 12245-73-7; $[C_6H_5CH_2NCH)Me_2]Cl$, 1875-92-9; Ir[$C_6H_3(CH_2NMe_2)$-2-Me-6](COD), 114762-90-2; Ir[$C_6H_3(CH_2NMe_2)$-2-CH_2NMe_2-6](COD), 114762-89-9; [1-($Me_2(H)NCH_2$)-3-Me-C_6H_4]Cl, 115031-97-5; [1,3-($Me_2(H)NCH_2)_2C_6H_4$]Cl_2, 63400-16-8; {$SnMe_2[C_6H_3(CH_2NMe_2)_2$-2,6]}Cl, 115092-11-0.

Supplementary Material Available: Tables of anisotropic thermal parameters and all H-atom parameters and a complete list of bond lengths and bond angles (7 pages); listing of observed and calculated structure factor amplitudes (46 pages). Ordering information is given on any current masthead page.

(30) Brookhart, M.; Green, M. L. H. *J. Organomet. Chem.* **1983**, *250*, 395.
(31) Periana, R. A.; Bergman, R. G. *J. Am. Chem. Soc.* **1986**, *108*, 7332.

Defect Patterns in Perovskites

Jeremy K. Burdett* and Gururaj V. Kulkarni

Contribution from the Chemistry Department, The University of Chicago, Chicago, Illinois 60637. *Received December 9, 1987*

Abstract: The method of moments is used to understand the results of molecular orbital calculations and tight-binding calculations on solids, designed to probe the reasons behind the ordering problem of defects in solids. This is a problem that can be regarded as the solid-state equivalent of the isomerization question in molecular chemistry. The structural preferences for *cis*- and *trans*-dioxo transition-metal complexes and the "defect patterns" predicted for binuclear vertex-sharing octahedral complexes of stoichiometry M_2L_9 are used to build a simple model that may be easily applied to the case of transition-metal-containing perovskites. The calculations and the model give a ready explanation for the observed ordering pattern in $CaMnO_{2.5}$ and defect structures with fewer oxygen vacancies.

One of the important aspects of the geometrical structure of molecules is, of course, the stability of isomers of various types. Rotational isomerism in organic chemistry and the relative stability of cis and trans isomers in transition-metal chemistry come immediately to mind. Often the stability of the two structures varies with electron count. For example, *cis*-dioxo complexes are exclusively found for d^0 metal centers but the trans isomer for d^2 systems. Often the predicted properties of the two isomers are very different, and this point underscores the often striking dependence of properties on structure. Seemingly minor geometrical variations often lead to very different properties.

Ordering patterns in molecules are important too. Given a collection of atoms that are to be assembled into a molecule of a set shape, what influences the choice of atomic connectivity? For example, in the structure of nitrous oxide, the oxygen atom is found in a terminal rather than central position. The most stable "coloring" pattern changes too with electron count. In the A_2O oxides, for molcules with 8-12 electrons (Li_2O, Ga_2O, for example) the oxygen atom is centrally located in contrast to the 16-electron case of N_2O.

In this paper we will study a problem of very basic chemical importance in the condensed phase. We will present a theoretical way to understand the ordering patterns of defects in solids. Our model will be applied initially to systems derived from the perovskites, materials of composition ABO_3.[1] Such defect structures give us a solid-state equivalent of the isomerism problem of the molecular chemist. Here we wish to understand what influences their relative stabilities. Throughout our analysis we shall make extensive analogies with molecular problems. The major thrust in this paper will be to understand the atomic arrangement in the material $CaMnO_{2.5}$ and other related systems with slightly higher oxygen content. Elsewhere we extend the picture to structures with lower oxygen content ($O_{2.33}$), which have recently been found to be high T_c superconductors.[2-4] We will use one-electron orbital models which have proven immensely useful in almost all areas of chemistry, and will find the method of moments especially useful in understanding the variation in structural stability with electron count.

Defects in $CaMnO_3$

The chemist's view of defect structures is one that has changed over the years.[5-7] Many of the structures, that carried this label years ago are now recognized as chemically distinct phases. If the number of defects is rather small (such as the Schottky defects

(1) Smyth, D. M. *Annu. Rev. Mater. Sci.* **1985**, *15*, 329.

(2) Wu, M. K.; Ashburn, J. R.; Torng, C. J.; Hor, P. H.; Meng, R. L.; Gao, L.; Huang, Z. J.; Wang, Y. Q.; Chu, C. W. *Phys. Rev. Lett.* **1987**, *58*, 908.
(3) Cava, R. J.; Batlogg, B.; van Dover R. B.; Murphy, D. W.; Sunshine, S.; Siegrist, T.; Remeika, J. P.; Rietman, E. A.; Zahurak, S.; Espinosa, G. P. *Phys. Rev. Lett.* **1987**, *58*, 1676.
(4) Schuller, I. K.; Hinks, D. G.; Beno, M. A.; Capone, D. W.; Soderholm, L.; Loquet, J.-P.; Bruynseraede, Y.; Segre, C. U.; Zhang, K. *Solid State Commun.* submitted for publication.
(5) A survey is given in Clark, G. M. *The Structures of Non-Molecular Solids*; Applied Science: London, 1972.
(6) West, A. R. In *Solid State Chemistry and Its Applications*; Wiley: New York, 1984; Chapters 9 and 10.
(7) Rao, C. N. R.; Gopalakrishnan, J. In *New Directions in Solid State Chemistry*; Cambridge University Press: Cambridge, 1986; Chapter 5.

0002-7863/88/1510-5361$01.50/0

in NaCl), and not highly ordered, then we now regard the material in a different light to one that contains a significant percentage of ordered vacancies. A set of examples of the latter type might be the titanium oxides where each material has a distinct crystal structure related by a crystallographic shear (CS) operation to the parent.[8] In wüstite (FeO) the defect structure probably gives rise to clustering of Fe atoms[9] arranged on tetrahedral sites (a Koch cluster) rather than the octahedral sites of the parent rocksalt structure. The materials that we shall study here are systems, where in the so-called "defect" structure, the cation sites are only partially occupied with respect to some parent. A material such as alumina is in principle a defect structure of this type[5] in that the octahedral holes of the close-packed oxide array are only two-thirds occupied by metal ions. In this paper we shall study the series of defect perovskites $ABO_{2.5}$[10,11] simply related[10] to the parent ABO_3 by the selective removal of oxide ions. $CaMnO_{2.5}$ has been studied by neutron and X-ray diffraction and a distinctive ordering pattern identified. $CaMnO_3$ itself is an interesting catalyst[12-14] that contains readily removable (and thus chemically potent) oxygen. The quaternary oxides of copper,[2-4] shown recently to be high-temperature superconductors, also have very mobile oxygen atoms.

1 shows a polyhedral picture of the parent structure, where each B atom is octahedrally coordinated by oxygen, and **2** the generation of square-pyramidal BO_5 units by oxygen deficiency. (Many

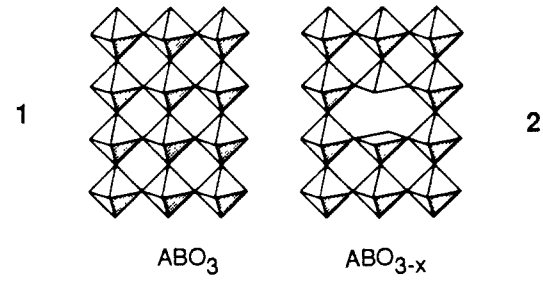

distorted and nonstoichiometric perovskites exist, as well as superstructures such as that of cryolite). Not all defect materials give rise to equivalent metal coordination sites even with the same stoichiometry. $CaFeO_{2.5}$ with a high-spin d^5 electron configuration is also a defect perovskite, but has the brownmillerite[15] structure. Here the distortion pattern is one that involves the formation of cis vacancies around half of the metal atoms which relax to give locally tetrahedral structures. The other metal atoms are octahedrally coordinated.

The actual pattern of vacancies in $CaMnO_{2.5}$ is the one derived from a perovskite sheet as shown in **3**, but what is wrong with the alternative ordering of **4**? Both of them have identical local environments in that they give rise to square-pyramidal coordination at all the metal sites. Our answer to this question will start by looking at a problem mentioned in the introduction. We will have much to learn from understanding the relative stability of the cis and trans isomers of transition-metal dioxo compounds.

cis- and *trans*-Dioxo Compounds

Without exception, all d^0 transition-metal (excluding the actinides) dioxo compounds have the cis, and all d^2 examples, the

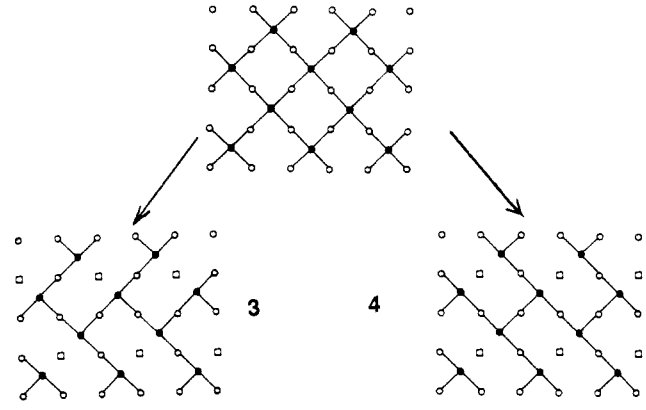

trans arrangement. Molecular orbital diagrams can be constructed very easily for the two by using the angular overlap model[16] and are shown in **5**. Just as the organic chemistry draws molecular

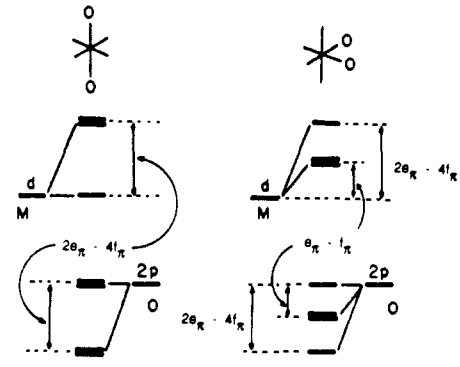

5

orbital diagrams for benzene that include only the π network, we only show here the collection of metal d and oxygen p orbitals involved in π bonding. The presence of an underlying σ framework is implied. The difference in energy between the two isomers as a function of π electron count is shown in **6**. (Since there is one

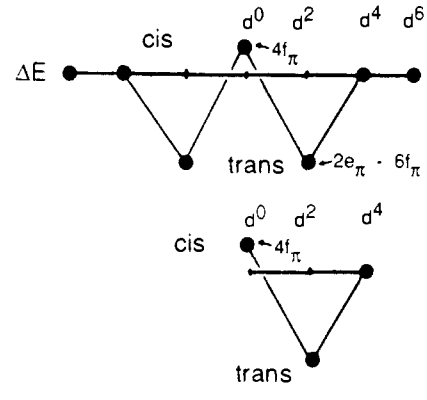

6

nonbonding oxygen p orbital common to both structures, its filling is ignored.) The plot is in accord with the experimental observations, namely the two points at d^0 and d^2. Many of the electron counts are chemically unrealistic. Those with partially filled oxide levels are meaningless, since in all compounds of interest there is a formal charge transfer to oxygen of two electrons. In addition there are other oxygen levels, those that are involved in σ bonding, in this region as well. We show in addition, therefore, just that part of the curve which will be useful to us. The *shape* of the *overall* curve however is one that will allow great insight into the orbital problem as we will show. Notice that a very simple theoretical model gives us this result. At this point it is pertinent to remind the reader of the relative sizes associated with the angular overlap parameters e_σ and e_π. In general, the interaction

(8) For example, see: Ostrowetsky, S. *Bull. Soc. Chim. Fr.* **1964**, *1012*, 1018.
(9) Roth, W. L. *Acta Crystallogr.* **1960**, *13*, 140.
(10) Poeppelmeier, K. R.; Leonowicz, M. E.; Longo, J. M. *J. Solid State Chem.* **1982**, *44*, 89.
(11) Poeppelmeier, K. R.; Leonowicz, M. E.; Scanlon, J. C.; Longo, J. M.; Yellon, W. B. *J. Solid State Chem.* **1982**, *45*, 71.
(12) Reller, A.; Jefferson, D. A.; Thomas, J. M.; Beyerlein, R. A.; Poeppelmeier, K. R. *J. Chem. Soc., Chem. Commun.* **1982**, 1378.
(13) Reller, A.; Jefferson, D. A.; Thomas, J. M.; Uppal, M. K. *J. Phys. Chem.* **1983**, *87*, 913.
(14) Voorhoeve, R. J. H. In *Advanced Materials in Catalysis*; Burton, J. J.; Garten, R. L., Eds.; Academic: New York, 1975; p 129.
(15) Bertaut, E. F.; Blum, P.; Sagnieres, A. *Acta Crystallogr.* **1959**, *12*, 149.
(16) Burdett, J. K. *Molecular Shapes*; Wiley: New York, 1980.

energy between two orbitals of λ (= σ, π, δ) type may be written as a perturbation expansion. The lead (second order in the overlap integral) term carries the units of e_λ and the smaller (fourth order) term units of f_λ.

A particularly powerful way to understand the shape of this curve comes from the method of moments,[17-25] which has been recently used to study several chemical problems.[17-22] We refer the reader to ref 17 or 22 for a more detailed exposition. Using the language of this approach, the shape of this plot is that which is expected for a fourth moment problem, namely one where the first disparate moment of the energy density of states (the π levels in this example) of the two structures is the fourth. Here is not the place to describe the approach in detail, but if the electronic density of states of two structures first differs at the n^{th} moment, then the energy-difference curve between them as a function of fractional orbital occupancy (empty, $0 \le x \le 1$, full) will often be one that has n nodes (including those at $x = 0, 1$). **7** shows the set of curves that result. The reader can readily extend these to higher n. It is always the structure with the larger n^{th} moment that is more stable for the lowest orbital fillings, which means for the case under discussion, that it is the structure with the larger fourth moment that is less stable at the half-filled point.

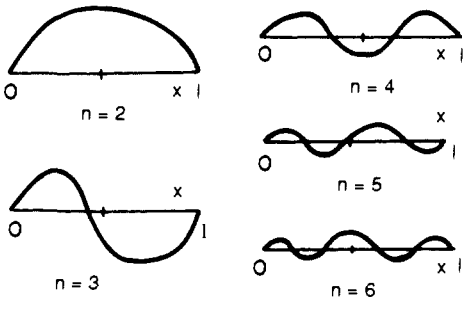

7

Use of the moments of a set of energy levels rather than the eigenvalues themselves is not the traditional way to look at chemical problems. However there is a very nice connection between geometrical structure and these moments which we shall find very useful indeed in this paper. Cyrot-Lackmann showed[23-25] that the n^{th} moment could be readily expressed (in Hückel theory at least) in terms of a topological index. This index is simply the sum of the weighted self-returning walks of length n in the orbital problem. Each step in the walk is weighted by the size of the interaction integral H_{ij} associated with each step linking a pair of orbitals.

For the present case, in order to correlate the moments of the energy density of states with elements of the geometrical structure, we need to evaluate the weights of all of the self-returning walks of length 4 from each orbital of the electronic problem. Recall that if two orbitals do not overlap, then H_{ij} is zero and the weight of that entire walk is zero. When viewing structural problems such as these, all we have to do in practice[17,22] is to see which walks are different in the two systems. For the dioxo compounds, while the two four-walks of **8** are found in the trans geometry, the one of **9** is the only contributor for the cis geometry. In other words, it is the trans arrangement that has the higher fourth moment (the larger number of four-walks) and thus is the least stable structure at the half-filled point. This is the electron count where

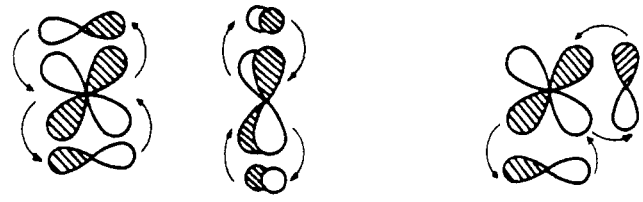

8 **9**

all the M–O π-bonding orbitals are filled and all the antibonding ones empty (i.e. the d^0 configuration). Notice that at the half-filled point the energy difference curve is controlled by the f_π parameter, which recall is much smaller than e_π. This is a general result. We often find that the amplitude of the various peaks in the plots of **7** vary considerably from system to system,[17] as does the exact location of the crossing points of the curve. In particular, as the electronegativity difference between the orbitals involved increases, the amplitude at the half-filled point decreases. As an illustration, we may directly compare the energetics of the curve of **6** with that for another fourth moment problem where there is no difference in electronegativity between the orbitals of the system. In twisted versus planar allene, an example of this type, a simple Hückel treatment, gives an energy difference of 1.18β at $x = 0.5$, and -0.82β at $x = 0.75$.

"Defect Molecules" of the Type M_2L_9

Here we wish to understand the relative stability of molecules with the geometries shown in **10–13** as a function of electron count.

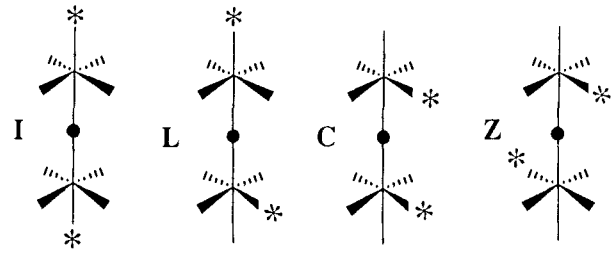

10 **11** **12** **13**

The molecules in **12**, **13** are simple rotational isomers and we shall often refer to them as a single species. We use an asterisk to represent a vacant site. There are several molecules of this type that contain planar porphyrin ligands. Here, however, the geometry is constrained[26] to be of the I type by the ligand rigidity. Unrestrained molecules of this type are quite scarce. In this study we will restrict ourselves to monatomic bridging ligands, which means we will exclude molecules such as Cu_2L_9(pyrazine). This species, containing d^9 Cu^{II} has an I-shaped structure. **14** shows the energy-difference curve we calculate for the possible species as a function of d count. We used Mn_2O_9 fragments as models

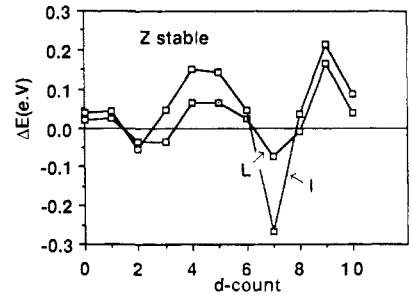

14

in our calculations. These were of the extended Hückel type with the parameters given in the Appendix. Using the results of the previous section, we can readily understand the shape of the

(17) Burdett, J. K. *Struct. Bonding (Berlin)* **1987**, *67*, 29.
(18) Burdett, J. K.; Lee, S. *J. Am. Chem. Soc.* **1985**, *107*, 3050.
(19) Burdett, J. K.; Lee, S. *J. Am. Chem. Soc.* **1985**, *107*, 3063.
(20) Burdett, J. K.; Lee, S.; McLarnan, T. J. *J. Am. Chem. Soc.* **1985**, *107*, 3083.
(21) Burdett, J. K.; Lee, S. *J. Solid State Chem.* **1985**, *56*, 211.
(22) Burdett, J. K. *Acc. Chem. Res.* **1988**, *21*, 189.
(23) Ducastelle, F.; Cyrot-Lackmann, F. *J. Phys. Chem. Solids* **1970**, *31*, 1295.
(24) Ducastelle, F.; Cyrot-Lackmann, F. *J. Phys. Chem. Solids* **1971**, *32*, 285.
(25) Cyrot-Lackmann, F. *J. Phys. Chem. Solids* **1968**, *29*, 1235.
(26) Tatsumi, K.; Hoffmann, R. In *Hemoglobin and Oxygen Binding*; Ho, C., Ed.; Elsevier: New York, 1982.

Table I. Missing Walks and Their Weights in **10–13**[a]

	weights of walks absent in:		
	10	**11**	**12, 13**
σ walks (units of S_σ^6)	$2(\sqrt{3}/6)^6 + 2.1^6$	$2(\sqrt{3}/6)^6 + 1^6 + 1^4(1/2)^2$	$2(\sqrt{3}/6)^6 + 2.1^4(1/2)^2$
relative missing weight	3/2	3/4	0
π walks (units of S_π^6)	4	3	2
relative missing weight	2	1	0

[a] We have assumed here that $H_{ij} \propto S_{ij}$ and have defined two overlap integrals, S_σ, S_π, which define the σ and π overlap of an oxygen p orbital with a lobe of z^2 and one of the dπ orbitals, respectively, for a given metal–oxygen distance. Thus the relative weights are proportional to the serial product of the H_{ij}. The first line in the entry for the σ part of the table represents "x^2–y^2" walks of Figure 1d,f, the second line the "z^2" walks of Figure 1e,g. The π part of the table represents the walks of Figure 1a,b,c.

energy-difference curve. Simply put, the energy difference between **10** and any of the other isomers, or between **11** and any of the other isomers, will be determined by the sixth moment since a walk of the type shown in **15** is absent in **11** and two such walks

15

are absent in **10**. We should look however at the walks connecting the orbitals in more detail for a more complete understanding of the structural problem. For the σ walks recall that for a fixed metal–ligand distance, overlap with the "collar" of z^2 is smaller than that with the lobe along z (by a factor of $-1/2$), and overlap with a lobe of x^2–y^2 is similarly smaller by a factor of $\sqrt{3}/2$. (A table of the angular dependence of overlap integrals is given in ref 16.) Since $H_{ij} \propto S_{ij}$, σ walks that involve z^2 and turn corners then have a smaller weight than walks that proceed in straight lines. Figure 1 shows the σ and π walks and Table I the weights of the various walks that are absent in the structures **10–12** in terms of the two types of overlap integral that define the electronic situation. (For simplicity we have not included in the σ part the "mixed" walks that involve x^2–y^2 at one center and z^2 at the other. The trend in their weights is in the same direction as the ones shown.) **12** is the structure with the largest weight and thus should be the arrangement disfavored at the half-filled point (d^0 for π and d^6 for σ).

This is in nice agreement with the calculated curves. Notice that there are two plots, basically of the same shape but one with a larger amplitude than the other, representing the π and σ parts of the problem. Smoothed out versions of the two halves of the plot of **14** are shown in **16** and **17** for easy comparison with those of **7**. The π and σ parts of this problem are separable in the

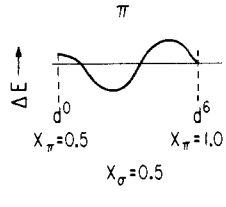

16

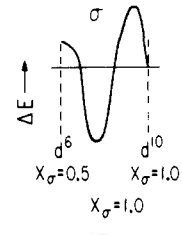

17

present case because the ligands lie along the Cartesian directions, and because in this particular system the "e_g" and "t_{2g}" blocks of levels are separated by an energy gap. As the d levels become occupied, first the M–L π^* levels are filled (d^0–d^6), followed by the M–L σ^* ones (d^7–d^{10}). There is a smaller amplitude for the π curve compared to its σ analogue, simply because of the smaller π compared to σ overlaps. We may emphasize the sixth moment

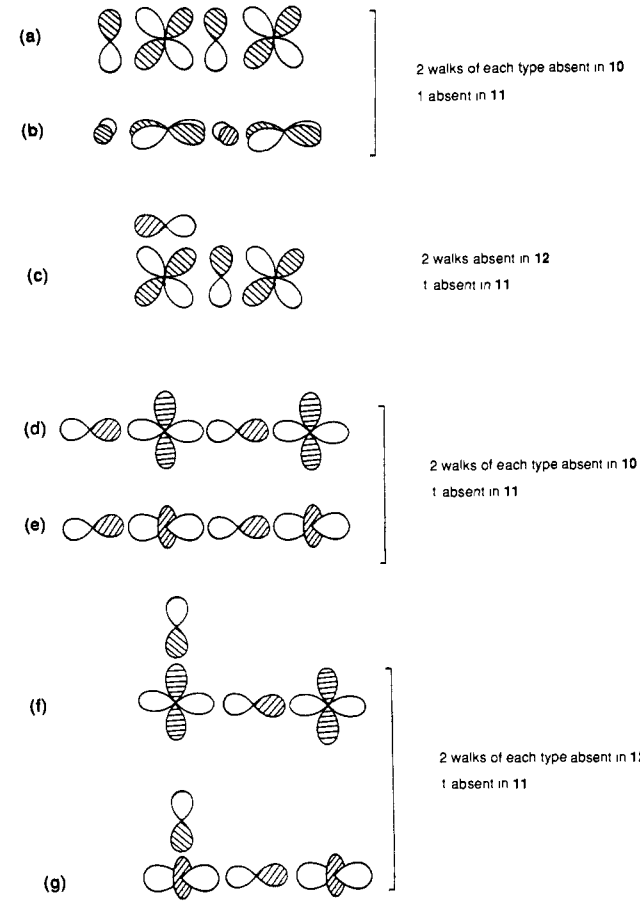

Figure 1. Walks to be counted in "defect" M_2L_9 molecules. For clarity only the orbitals between which the walks are made are shown here. It is a simple matter to add the arrows as in **8**, **9**.

character of the problem by connecting the σ part of **14** with its mirror image as in **18**. The six nodes are now apparent, as is

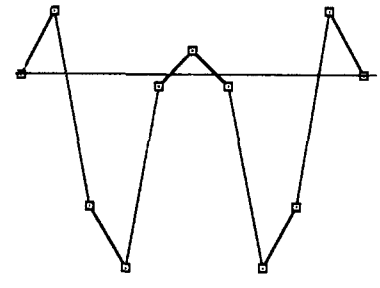

18

the rather small amplitude at the half-filled point, a feature we pointed out above for the dioxo compounds. As an aside we note that the energy-difference curve predicts the stability of the Z or C geometry at the d^9 configuration, rather than the I or L arrangement. There is of course an alternative way to view this result, and that is that octahedral, or pseudooctahedral, d^9 complexes are Jahn–Teller unstable and invariably either lose one or two trans ligands or have long bonds to these ligands. We have looked at the Jahn–Teller effect itself using the moments approach.[17] At a single metal center it is a fourth moment problem, but at two coupled centers it becomes a sixth moment one.

There are other structural problems that are very similar to those of isomer preference. Can we occupy these vacant sites in the molecule, either with atoms that have longer bonds and hence weaker (but not zero) interactions with the metal, or simply with atoms different in nature to oxygen? We replaced an O vacancy by an F atom in these materials to test out these ideas. Fluorine has a weaker σ and π interaction with the metal compared to oxygen, as shown by their e_σ and e_π parameters.[16] **19** shows the calculated energy difference curves for the various isomers, very

similar indeed to those of **14**. Here the labels Z, I, etc. refer to

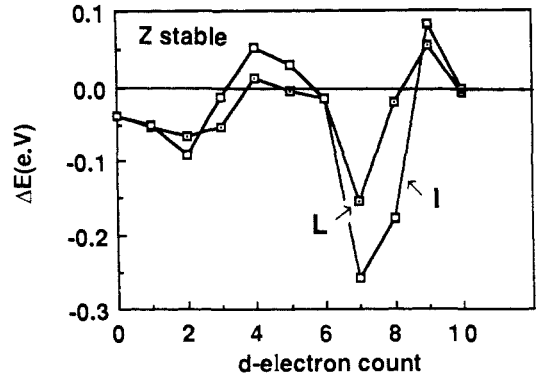

19

the fluorine atom location in $Mn_2O_9F_2$. This particular problem is thus analogous to the one mentioned earlier for nitrous oxide. The energy-difference curve we calculate for molecules containing longer bonds at the starred positions of **10–12** is similar too. We can reduce the overlap at a particular metal–ligand site too by bending the linkage off a Cartesian axis. A series of energy-difference curves with similar features arise here as well. Several of these structural aspects have not been studied experimentally for these molecules, but the general conclusions will be very important in allowing access to the solid-state problem described in the next section.

A comment concerning the application of these ideas to extended Hückel calculations is important to make at this point. For calculations of the Hückel type, where overlaps is ignored in the off-diagonal elements of the secular determinant, the energy-difference curve always has nodes at $x = 0, 1$. When overlap is included, then these cannot be guaranteed. In some problems we find an energy-difference curve with a strong sloping background, a result of a significant second moment contribution. In the present series of examples, the energy difference at d^6 is a composite of the energetic preference of the π manifold at $x = 1$ and that of the σ manifold at $x = 0.5$. We are lucky in this particular case too that σ/π separability occurs. If the "e_g" and "t_{2g}" bands overlap, then the energetic preferences in the overlapping region would be more difficult to analyze. In this case the transferability of the results from one metal to another and one ligand system to another will not be at all reliable.

Defect Perovskites of the Type $ABO_{2.5}$

Ordering of oxygen vacancies in perovskite type ABO_x metal oxides have been experimentally investigated[27] and superstructures are observed whenever there is ordering of vacancies. Highly ordered vacancy distributions have been identified in $ABO_{2.5}$ systems[10,11] and studied in detail,[30–33] but ordering is also found to occur at other points in the composition range ABO_x (x = 2.8, 2.75, 2.667).[28]

The energy-difference curve (per four Mn atoms) that we have calculated from our tight-binding band structure calculations (the parameters and details are given in the Appendix) for the two defect patterns of **3** and **4** is shown in **20** as a function of d count. It has a more complex shape than that for either of the two problems described above, but may be analyzed in a similar way.

The two colorings differ first at the eighth moment. This has to be the first disparate moment since for one vacancy to "see" another requires a self-returning walk of length eight. The curve shown in **20** only represents that part of the curve for $0.5 < x < 1.0$ (just as in the bottom half of **6**) and for two separate orbital problems, σ and π. It may be broken down into two individual

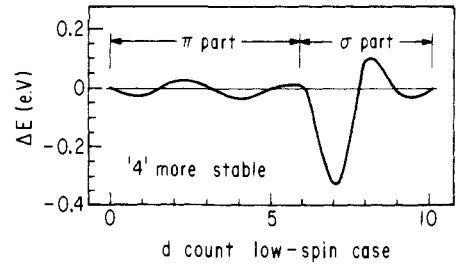

20

eighth moment plots as shown, one associated with the π (d^0–d^6) and the other associated with the σ (d^7–d^{10}) manifold. Just as the chemically important parts of **6** and **14** are associated with the occupation by electrons of the d orbitals so with the present case. The π and σ parts of the problem are separable for exactly the same reasons as described above for the M_2L_9 problem. Here we will focus on the σ part only. We can emphasize the eighth moment nature of the problem by using the same pictorial trick used earlier. **21** shows the result of adding the σ part of **20** to its mirror image. Now the eight nodes are apparent.

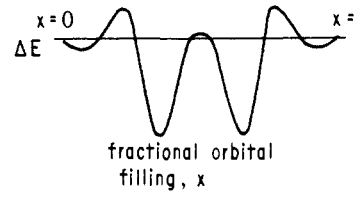

21

Where does this eighth moment originate in orbital terms? This is easy to see by tracing out the orbital pathways along the M–O–M linkages which make the two ordering patterns different just as we did before for the molecular problems. Since overlap with the "collar" of z^2 is smaller than with the lobe along z, we shall be able to extract the essence of the problem by considering straight walks only. In other words our walks should not turn corners. The walk of **22** is found in the arrangement **4**, but is not found (**23**) in the arrangement **3**. This comes about simply

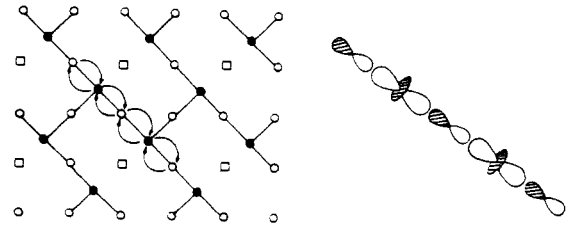

22

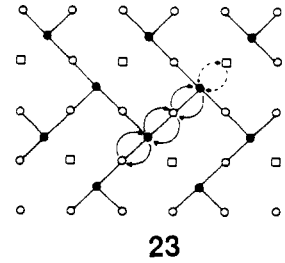

23

because of the infinite linear chains running through the arrangement **4** but only chain fragments in **3**. The eighth moment is the one that is important because this is the length of walk that first tells the middle atoms of the short fragment in **3** that they

(27) Grenier, J.-C.; Pouchard, M.; Hagenmuller, P. *Struct. Bonding (Berlin)* **1981**, *47*, 1.
(28) Reller, A.; Thomas, J. M.; Jefferson, D. A.; Uppal, M. K. *Proc. R. Soc. London, A* **1984**, *394*, 223.
(29) Wheeler, R. A.; Whangbo, M.-H.; Hughbanks, T.; Hoffmann, R.; Burdett, J. K.; Albright, T. A. *J. Am. Chem. Soc.* **1985**, *108*, 3083.
(30) Vidyasagar, K.; Gopalakrishnan, J.; Rao, C. N. R. *Inorg. Chem.* **1984**, *23*, 1206.
(31) Rao, C. N. R.; Gopalakrishnan, J.; Vidyasagar, K.; Ganguli, A. K.; Ramanan, A.; Ganapathi, L. *J. Mater. Res.* **1986**, *1*, 280.
(32) Vidyasagar, K.; Ganapathi, L.; Gopalakrishnan, J.; Rao, C. N. R. *J. Chem. Soc., Chem. Commun.* **1986**, *449*.
(33) Rao, C. N. R.; Gopalakrishnan, J. *Acc. Chem. Res.* **1987**, *20*, 228.
(34) Poeppelmeier, K. R., private communication.

are a part of a fragment rather than an infinite chain. As a result, the structure **4** has the larger eighth moment. From the development of the plots of **7** this means that **4** is the less stable structure at the half-filled point, but will be the more stable structure just after the half-filled point. This is just what we calculate in **20**. Notice the similar small amplitude behavior in **21** at $x = 0.5$ to that found in the molecular problems.

How do these results tie in with experiment? The $CaMnO_{2.5}$ example noted above contains a high spin Mn^{III} atoms. The plots we have shown map out the energetic behavior as the orbitals are filled with paired electrons and directly mimic the form of the electronic density of states. They therefore correspond to low-spin situations only. In the present case, calculation of the "high-spin plot", shown in **24**, is straightforward from the calculated electronic

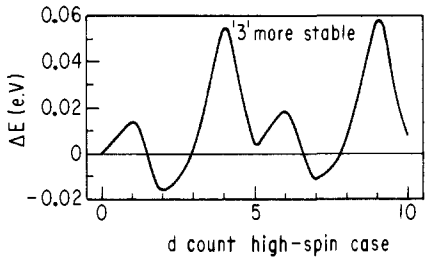

24

density of states and shows that the observed structure for $CaMnO_{2.5}$ is indeed the one predicted to be of lower energy. The shape of the energy-difference curve for these situations is not immediately understandable using the moments method, but we may readily understand the result for high-spin Mn^{III} (d^4) since it contains a single "e_g" electron. Since the energy preferences of the "t_{2g}" bloc are small, its energy preference will be similar to that for low-spin d^8. It is important to note that although our calculations indicate a greater relative stability for pattern **3** at the Mn electron count, it does not rule out the possibility of formation of vacancy pattern **4** or any other type of ordering, consistent with the stoichiometry and of low energy. In fact, minor domains of vacancy patterns other than **3** are observed[14] in $CaMnO_{2.5}$ along with the major portion of the material consisting of pattern **3**. In addition the pattern **4** has sometimes been identified crystallographically.[33] Experimentally and theoretically, however, **3** is of lower energy.

At this point one might ask if it is possible to predict the oxygen vacancy patterns in the composition range $CaMnO_x$; $2.5 \leq x \leq 3.0$ in general. In fact, phases such as $CaMnO_{2.667}$, $CaMnO_{2.75}$, and $CaMnO_{2.8}$ have been recently identified.[14] **25** shows the

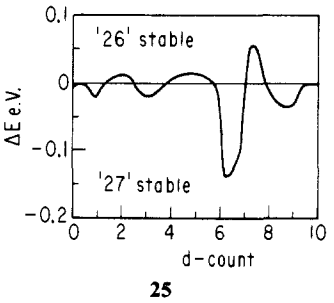

25

calculated energy difference curve corresponding to two possible vacancy patterns, **26**, **27**, for the phase $CaMnO_{2.667}$. These

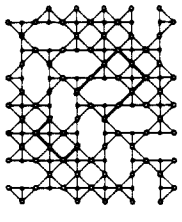

26

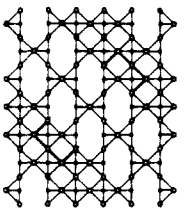

27

arrangements consist of a 1:2 mixture of 6-coordinate octahedral (high-spin d^3) and 5-coordinate square-pyramidal (high-spin d^4) Mn atoms with an average d-electron count of 3.667. **25** is an eighth moment curve and is very similar to that of **20**. Since the structural preference of the high-spin $d^{3.667}$ configuration should be similar to that of low-spin $d^{7.333}$, we expect the pattern **26** to be quite strongly favored compared to **27**. Experimentally,[14] it is not clear which pattern (**26** or **27**) is more stable or predominant. **28** and **29** show two possible vacancy patterns for the stoichiometry $CaMnO_{2.75}$. This phase contains a 1:1 mixture of octahedral and

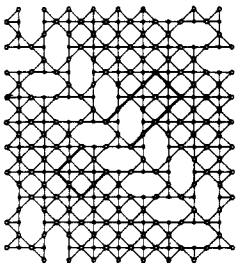

28

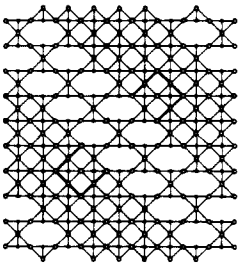

29

square-pyramidal Mn atoms, giving an average d-electron count of $d^{3.5}$. Our calculated energy difference curve, shown in **30**, which

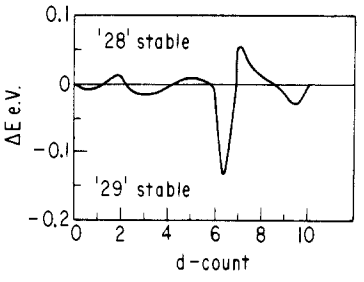

30

connects the patterns **28** and **29**, shows a preference for the pattern **28** for the high-spin configuration $d^{3.5}$ (or low-spin $d^{7.0}$). Experimentally, pattern **28** is found[14] to be the predominant phase, in agreement with theory. Very similar energy-difference curves are found for other pairs of vacancy patterns for the phase $CaMnO_{2.75}$. The movement in the maxima in the ΔE versus d^n curves **20**, **25**, **30** from higher to lower d counts ($d^{7.0}$ in $CaMnO_{2.5}$, $d^{6.33}$ in $CaMnO_{2.667}$, $d^{6.25}$ in $CaMnO_{2.75}$) is simply associated with increase in the ratio of octahedral to square-pyramidal metal ions along the series:viz., 0:1; 0.5:1; 1:1. The overall shape of the curve is, however, quite similar.

We can extend these results in principle to the homologous metal oxides AMO_x where the atomic configuration at the metal is different. Now A = Ca, La; M = Fe, Co, Ni, etc. Some of these materials are known[30-32] experimentally for $x = 2.5$, namely $CaFeO_{2.5}$ (d^5), $LaCo^{II}O_{2.5}$ (d^7), $CaCo^{III}O_{2.5}$ (d^6), and $LaNiO_{2.5}$ (d^8). Our approach is a valid one provided the defect pattern generates a structure where all metal atoms are in square-pyramidal coordination. Other than $CaCo^{III}O_{2.5}$ (d^6),[33] however, the existing experimental observations indicate a mixture of octahedral and square-planar (or tetrahedral) metal coordination for these oxygen-deficient metal oxides. For the Co^{III} case **3** is predicted, in agreement with experiment, irrespective of whether the metal is in the high- or low-spin configuration, but rather weakly. Thus direct comparison with experiment for several of these cases is not possible, but in view of the known high mobility of oxide ions in these materials, it is conceivable that under certain conditions 5:5 type square-pyramidal coordination may well become stabilized. In this case our results play a predictive role.

The relative importance of the several factors that control the local coordination numbers of these materials are more difficult to predict. For example the high-spin d^4 configuration is electronically acceptable for a square-pyramidal geometry, but not for a mixture of square-planar and octahedral coordination, since in the latter a Jahn-Teller instability results. This may be removed, however, by changing the spin state from high to intermediate spin. In other cases it is quite obvious that we should assign different oxidation states to the metal atoms in the different coordination geometries. The mixed-valence Pt^{II}/Pt^{IV} system we

describe later is a case in point. The balance of one- and two-electron terms in the energy has always been a problematic one to really predict for a given species. The moments approach has thus been very successful in tackling only one part of this problem. It would be more difficult and much more involved to explain this preference in more conventional language. As an indicator of the interpretive problem, Figure 2 shows computed electronic densities of states for the two defect patterns of **3** and **4**. They are quite similar.

Solid Solutions

The method used above should be a useful way to view defect patterns in a variety of materials to reach an understanding of the factors that control these arrangements in terms of what are rather simple orbital considerations. It can also be used to look at solid solutions. The two colorings of **3**, **4** have vacancies where there are obviously no bonds to the metal from these sites. Can we occupy these sites either with atoms that have longer bonds and hence weaker (but not zero) interactions with the metal or simply with atoms different in nature to oxygen as in the molecular isomer problem above? **31** shows our calculated energy difference

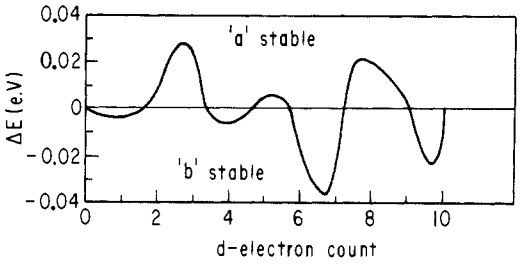

31

curve for the two species $ABO_{2.5}F_{0.5}$. Apart from a scale factor in the amplitude of the curve, it is very similar to that of **20**. Experimentally it is difficult to distinguish between a random and ordered structure because of the similar scattering power of O and F by X-rays. In this area then our results are predictive. We suggest too that when the amplitude of the curves of **20** and **31** is small, the energetics controlling the ordering patterns in perovskites will be small, so that entropic considerations could well dominate, giving random substitution patterns.

Distortions of Perovskites

Many of the perovskites and cryolites are distorted away from the regular cubic structure by bond stretching and contraction. We have already studied[29] some aspects of this problem for low d counts. Here we use the moments approach to view this problem. Structures **33–35** show three possible geometrical distortions relative to the cubic perovskite structure **32**. **33** represents a 6:4

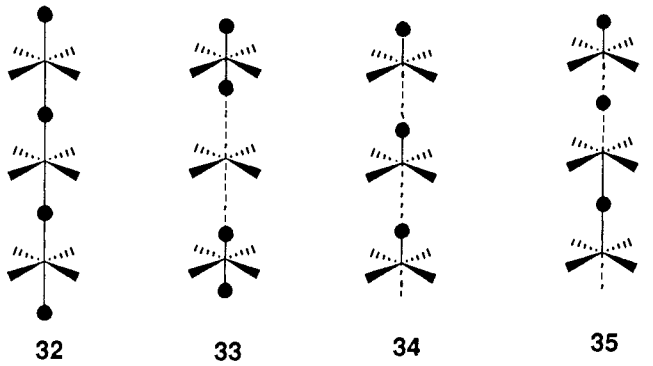

32 **33** **34** **35**

type of distortion that alternates pairs of short and long M–O distances along one of the Cartesian directions of the ideal perovskite structure and gives rise to alternate square and octahedral metal coordination. A one-dimensional example of this problem is that of the well-known mixed-valence compounds of platinum.[35,36] These materials contain Pt^{II} and Pt^{IV} and have an

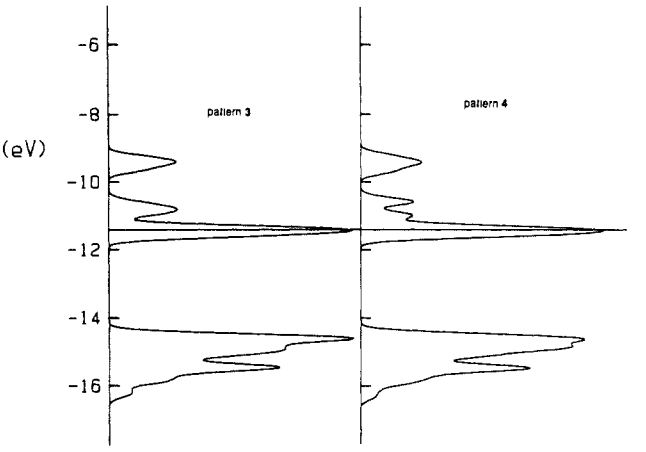

Figure 2. Computed electronic density of state for the two defect patterns **3** and **4** of $CaMnO_{2.5}$.

Table II

atom	orbital	H_{ii}, eV	ζ_1[a]
O	2s	−32.30	2.275
	2p	−14.80	2.275
Mn	4s	−9.75	1.800
	4p	−5.89	1.800
	3d	−11.67	2.800

[a] Slater-type orbital exponents.

average d count of 7. There are long and short distances in the perovskite $Cs_2Au_2Cl_6$, where the average d count is 9. Recently, the structure of $LaNiO_{2.5}$ has been found to contain Ni in 6-coordinate octahedral and 4-coordinate square-planar sites with an average d electron count of 8. The calculated energy difference curve, **36**, connecting the parent cubic structure and the distorted

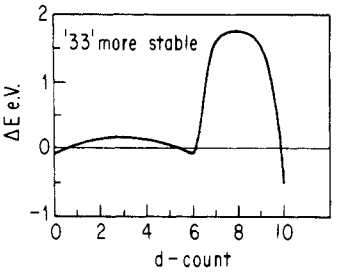

structure **33** is in accord with these observations. The distorted structure **33** is indeed predicted to be strongly stabilized for materials with electron counts 7–9. At higher band fillings the distorted structure **33** is favored not only with respect to the parent cubic structure but also relative to the other distorted variants **34** and **35**. The prediction of the 6:4 structure for the d^7 configuration is very easy to understand in local terms. A square-planar geometry is just what we would expect for a low-spin d^8 system, and the octahedral structure is quite appropriate for a low-spin d^6 configuration.

The plot **36** is clearly a fourth moment curve (see **7**), as we should expect, although there is no node at the d^{10} configuration. The two trans oxygen atoms first "see" each other via walk of length four. Thus this problem is of the same order as the Peierls distortion in solids and the Jahn-Teller distortion in molecules and indeed can be given such a label here too. The form of the curve between d^6 and d^{10} is very similar to the one shown in ref 17, which describes the Jahn–Teller distortion abouut a single octahedrally coordinated transition metal center, and was derived by using the angular overlap model. The major difference between the two is that here the energy-difference curve does not have a node at d^{10}, a result of the inclusion of overlap into the orbital problem here but not earlier. Topologically the state of affairs is very similar to the question of the relative stability of the cis and trans

(35) Whangbo, M.-H.; Foshee, M. J. *Inorg. Chem.* **1981**, *20*, 113.

(36) Whangbo, M.-H. *Acc. Chem. Res.* **1983**, *16*, 95.

transition-metal dioxides discussed above. They are both fourth moment problems when phrased in this language.

37 shows the energy-difference curve for the pair of distorted structures **34** and **35**. It is again a fourth moment curve but with

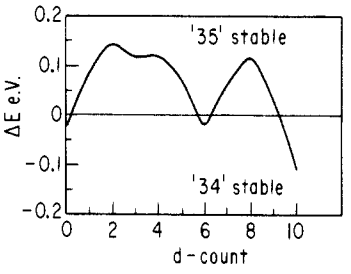

prominant π as well as σ parts. Notice that the distortion pattern **35** containing elongated M···O···M bonds is favored for all d counts other than 0, 6, and 10. It is reasonable to assume that these O atoms in the elongated M–O–M linkages are the ones that are lost on reduction of the material. This gives us an electronic reason why $CaMnO_3$, on reduction to $CaMnO_{2.5}$, should lead to MnO_5 square pyramids arranged face to face as in **35** rather than back to face as in **34**. It is very instructive to see how the fourth moment curves arise in these problems. It is easy to see from **38** and **39** that self-returning walks of length 4 may involve both long bonds, both short ones or one short and one long. The contribution to the fourth moment (per M–O–M–O–M unit) which involves walks over more than one linkage is simply $4l^2s^2$ in **38**. In **39** the corresponding weight is $2l^2s^2 + l^4 + s^4$ or $4l^2s^2 + (l^2 - s^2)^2$. Here l and s represent the H_{ij} values for the long and short bonds in the structure. It is easy to see that the fourth moment will always be larger in **39** ($(l^2 - s^2)^2$ will always be positive) and thus the structure stable at the half-full point (d^6 and d^{10}) should be **35**, in accord with our plot of **37**.

There is another striking result that comes out of analyses of this type. Notice that in contrast to the energy difference curves encountered earlier (e.g. **20**, **25**, **30**) the π part of the curve in **37** is energetically quite important, and in fact seems to be as strong as that associated with the σ part. The reason is again quite simple. There are an equal number of short and long M–O distances in **34** and **35**, and in both geometries the O–O distances

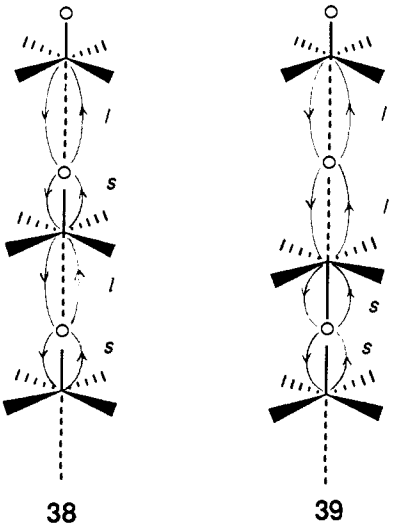

38 **39**

are equal too. However, the M–M distances are not the same in the two structures. While **35** has equal numbers of short and long distances, **34** has but a single intermediate distance. The shorter M–M distances in **35** lead to stronger direct $d\pi$–$d\pi$ interactions here and a second moment contribution to the energy difference curve, which always favor this structure for $d\pi$ orbital fillings.

Acknowledgment. This research was supported by the National Science Foundation under NSF DMR8414175 and by the donors of the Petroleum Research Fund, administered by the American Chemical Society. We thank Prof K. R. Poeppelmeier for some useful conversations.

Appendix

The calculations were performed by using the extended Hückel method for both the molecular orbital calculations on molecules and the tight-binding band structure calculations for solids. The parameters used are given in Table II. Typically 24K points were used in the irreducible wedge of the Brillouin zone for the band structure computations.